Model-based design for self-sustainable sensor nodes

Philipp Mayer [a],[*], Michele Magno [b], Luca Benini [a],[c]

[a] *Integrated Systems Laboratory, ETH Zurich, Zurich, 8092, Switzerland*
[b] *Center for Project-Based Learning, ETH Zurich, Zurich, 8092, Switzerland*
[c] *Department of Electrical, Electronic and Information Engineering, University of Bologna, Bologna, 40136, Italy*

ARTICLE INFO

ABSTRACT

Long-term and maintenance-free operation is a critical feature for large-scale deployed battery-operated sensor nodes. Energy harvesting (EH) is the most promising technology to overcome the energy bottleneck of today's sensors and to enable the vision of perpetual operation. However, relying on fluctuating environmental energy requires an application-specific analysis of the energy statistics combined with an in-depth characterization of circuits and algorithms, making design and verification complex. This article presents a model-based design (MBD) approach for EH-enabled devices accounting for the dynamic behavior of components in the power generation, conversion, storage, and discharge paths. The extension of existing compact models combined with data-driven statistical modeling of harvesting circuits allows accurate offline analysis, verification, and validation. The presented approach facilitates application-specific optimization during the development phase and reliable long-term evaluation combined with environmental datasets. Experimental results demonstrate the accuracy and flexibility of this approach: the model verification of a solar-powered wireless sensor node shows a determination coefficient (R^2) of 0.992, resulting in an energy error of only -1.57% between measurement and simulation. Compared to state-of-practice methods, the MBD approach attains a reduction of the estimated state-of-charge error of up to 10.2% in a real-world scenario. MBD offers non-trivial insights on critical design choices: the analysis of the storage element selection reveals a 2–3 times too high self-discharge per capacity ratio for supercapacitors and a peak current constrain for lithium-ion polymer batteries.

1. Introduction

Pervasive wireless sensors are building the interface between the physical and digital worlds. Thus, they are considered key building blocks for Industry 4.0 [1]. These devices enable environmental data collection in countless applications, from simple periodical temperature logging to autonomous embedded condition monitoring of industrial machinery [2]. One of the main obstacles of such sensing devices to become truly pervasive is their need for a long-term reliable power source. Batteries are the main and obvious way of powering wireless devices, but regular battery replacement or recharging is vital to ensure longtime operation. Such a requirement implies high maintenance costs, especially if devices are poorly accessible or if environmental issues related to battery disposal are of concern [3]. These aspects are getting even more substantial in applications where devices are deployed on a large scale [4].

Energy harvesting (EH), namely the utilization of environmental energy sources for powering wireless sensors, is the most promising technology to prolong maintenance-free lifetime. EH has been the subject of intensive research for more than one decade and has been demonstrated in several highly successful applications. However, many research questions are still open for small-sized harvesters needed for low-cost and unobtrusive devices [5]. EH for miniaturized wireless sensors requires additional circuitry for energy management and power conversion from low-power and low-voltage compact EH transducers. Thus, despite continuous improvements in circuit energy consumption and integration, opting for EH inevitably results in increased device cost. This drawback can be compensated to a certain extent under consideration of the total cost of ownership if a maintenance-free operation can be guaranteed [6]. However, relying on fluctuating and deployment-specific environmental energy in a commercial product makes it challenging to guarantee reliable operation over the marketed time horizon [4]. In fact, this uncertainty hinders the spreading of EH as it can ultimately result in brand damage or product liability. Thus, methods and techniques are required to assess the longtime behavior of EH-powered devices reliably.

Model-based design (MBD), which has been among other fields successfully applied in the automotive [7] and aerospace [8,9] domain, has the potential to address this need. MBD emphasizes mathematical

Table 1
Comparison to embedded systems works targeting virtual prototyping.

	MSSP'18 [12]	LCA'18 [13]	NEWCAS'15 [14]	MBMV'20 [15]	this work
Scope	energy harvester	intermittent computing	embedded system	embedded system	EH powered embedded system
Environment	MATLAB SIMULINK	analytical model	SystemC-AMS	SystemC-AMS	MATLAB SIMULINK
Model	harvester	load	battery, load	battery, load	harvester, energy management, battery, load
Abstraction	low	very high	high	high	medium

modeling to design, analyze, verify, and validate systems [10]. A complete model of a self-sustainable system comprises its coupling with the environment, physical processes in the energy conversion, energy management, and embedded computation and communication. Based on the system model, the behavior may be tested and simulated offline, enabling developers to verify design decisions and to analyze longtime reliability or the response in the event of a fault [11].

This work aims at leveraging the potential of a model-based design approach in the context of small-sized wireless sensor nodes powered by energy harvesting. The proposed development process combines environmental energy data with a circuit-specific power balance model to allow long-term analysis. By extending existing dynamic models combined with data-driven statistical modeling of state-of-the-art EH converters, circuit modeling accuracy is significantly improved without implying an increase in model complexity. This is achieved by modeling the dynamic conversion efficiency of the power path. Model reuse and substitution are facilitated by splitting the sensor node model into elementary circuit blocks, allowing a comparison of different EH transducers, harvesting circuits, and storage element chemistries. This work presents four main contributions:

1. The formulation of an accurate and complete system model, including blocks for energy harvesting transducers, power conversion and management circuits, and energy storage elements.
2. The demonstration of the applicability of data-driven regression-based modeling to accurately emulate state-of-the-art commercial energy harvesting converters.
3. A verification of the proposed system model based on extensive lab experiments demonstrating a coefficient of determination (R^2) of 0.992 and an energy error of -1.57%.
4. An exemplary demonstration of the advantages of the MBD approach to identify optimization potential and analyze long-time behavior, including a comparison to the state-of-practice assessment method.

The rest of the article is organized as follows: Section 2 discusses related work and limitations of current methods; Section 3 sketches the MBD flow for EH powered sensors; Section 4 describes the system architecture and the design of the individual simulation blocks; Section 5 reports on experimental verification of the simulation model followed by an exemplary analysis of the longtime self-sustainability and optimization of an autonomous wireless sensor node; Finally, Section 6 concludes the paper.

2. Related work

The research on the design of self-sustainable devices has been prolific in the last decade, with a vast number of EH-powered sensors covering highly application-specific tasks from indoor air quality monitoring [16] to powering wearables with the human body heat [17]. Surveys on wireless sensor nodes powered by energy harvesting with an overview of EH transducers, circuit topologies, energy storage technologies, and algorithms are given in [3,18]. A common requirement in EH system design is to match source and load power points: this is achieved with energy storage capacity selection during design [19] or with energy-aware load management during runtime [20,21]. In addition to this temporal matching, there is the requirement for power matching to maximize the extracted energy [22]. Matching is particularly crucial for

small-sized harvesters with an output power of a view microwatts that need to supply wireless sensor nodes with peak power of milliwatts. Finally, there is not only the requirement to study and optimize the circuitry itself but also to precisely analyze the application-specific energy statistics to ensure long-term reliability [23]. A resilient power path design capable of overcoming temporary absences of environmental power, e.g., with cold start circuitry, allows to partially circumvent this critical design point but does not ensure continuous availability [24]. If short-term system interaction with the environment has to be analyzed, environmental testbeds, such as presented in [25], can be used. However, for observation periods from several weeks to years, such test setups are inconvenient and inevitably require an analytical approach. Such an analysis can be performed at different levels of complexity, from a static calculation of the system behavior in known environmental conditions to heterogeneous models, including multi-physics models and formal models of computation [10]. For model-based analysis, the interdisciplinarity and complexity make the description of EH-powered wireless sensor nodes – and cyber–physical systems in general – challenging. This is reflected in previous research works, where the predominant number of publications focuses on modeling only some elements in the power path, e.g., energy harvesting transducers [12,26–29] elements [30–32], or the workloads, e.g., computation or communication [13]. However, the full potential of model-based design is realized only with a holistic system-level model [33].

A high-level comparison of works targeting virtual prototyping for embedded systems is given in Table 1. [12] demonstrates the advantages of modeling to optimize EH transducers and estimates their harvesting potential. Miguel et al. [13] analytically described the energy balance of EH-powered intermittent systems, illustrating the importance of a deep understanding of the interaction between computational load and available energy. A few works successfully utilized SystemC-AMS-based models in the design process of sensor nodes. [14] implemented an alkaline battery model and an application-specific load state-machine to estimate the battery lifetime of a wireless sensor node. With a similar concept, Heller et al. [15] simulated and optimized the power path of a deep brain stimulation implant. Although SystemC-AMS is highly versatile and computationally efficient, the presented work based on MATLAB SIMULINK has distinct advantages in terms of usability due to comprehensive and feature-rich existing models from MATHWORKS as well as better integration of custom EH transducers due to inherent multi-physics support.

In contrast to previous works, the aim of the proposed approach is not a mathematical description of stand-alone sub-systems but an accurate approximation of the complete power path of EH-powered sensor nodes. This allows a more holistic view of the system efficiency, e.g., a highly optimized EH transducer does not necessarily result in an efficient operation of the converter circuitry, and an analysis of the system performance over years of operation. To the best of our knowledge, this is the first complete EH-powered sensors model, reducing the energy error to just -1.57%, thereby enabling reliable long-term assessment.

3. Background

An agile model-based design process applied on an EH-powered wireless sensor node is depicted in Fig. 1. Starting from a requirement definition, including functional, technical, lifetime, and environmental
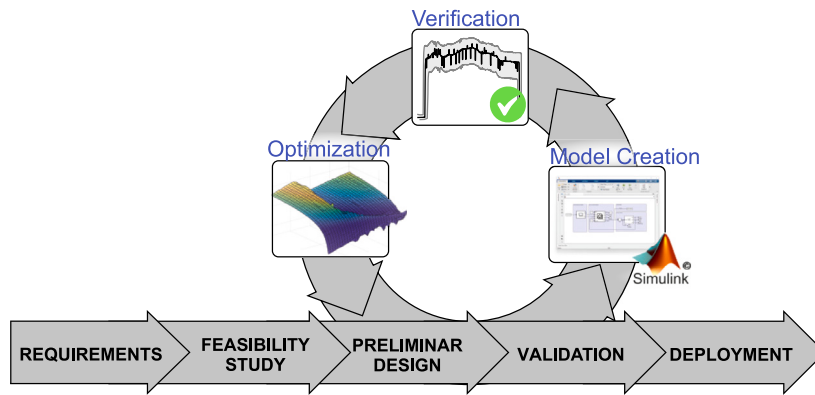
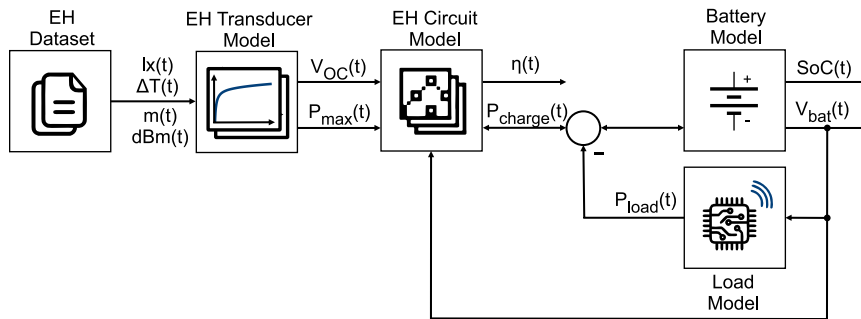**Fig. 1.** Agile model-based EH system design flow.

Fig. 2. High-level overview of the system model.

aspects, one or more EH sources are selected. Based on that, a preliminary analysis with a feasibility study is conducted, giving first insights into the applicability of energy harvesting in the targeted scenario. Subsequently, an initial virtual prototype is designed. This includes a preliminary definition of key system parameters and components, e.g., targeted EH transducer, circuit topology, storage element chemistry, wireless system on chip, etc., and the mathematical modeling of the individual components. Afterward, a physical prototype is created and analyzed in lab conditions to verify the designed model. The full model allows an in-depth analysis and optimization of the design based on simulation. Finally, the optimized and tested prototype is validated against the original requirements before being deployed or adapted in an additional development cycle.

4. System model

Despite the great variety of industrial and academic systems powered by energy harvesting, the underlying topologies bear significant similarities. These circuits consist mainly of an EH transducer, a voltage conversion circuit, intermediate energy storage, and an application-specific load. The unique characteristic of the individual systems come primarily from their application and the degree of coupling between source and load power points [3].

The following subsections discuss the proposed model design of the key system components, shown in Fig. 2. The implementation, which has been done as a multi-domain MATLAB SIMULINK model, aims to balance system complexity and accuracy while allowing the analysis of the system behavior with substitutable circuit blocks. The simplified model describes the circuit characteristics based on the power transfer between individual blocks under consideration of the voltage conversion ratios and efficiencies.

Table 2
Datasets for energy harvesting from commonly used environmental sources.

Energy harvesting source	Reference
Light	[34], [35]
Thermal gradient	[36], [37]
Vibration	[23], [38], [39]

4.1. Energy harvesting transducer model

To benefit from the model-based design approach for an EH-powered system, a comprehensive database on the environmental conditions in the targeted application is essential. An overview of the limited available datasets for the most common energy sources, light, thermal gradient, and vibration, is given in Table 2. The EH transducers can be described with multi-physics models, e.g., finite element method (FEM) models, based on the underlying physical phenomena as summarized in [12]. This allows an accurate simulation and optimization during the design phase of custom energy harvesting transducers. However, with high computational requirements, this low level of abstraction is not necessarily expedient for the analysis of the full EH-powered sensor node when combined with extensive environmental datasets.

From a circuit design perspective, the EH transducer can be described as a time-dependent non-linear voltage source. Under the assumption of a matched load, which is valid for maximal power point tracking (MPPT) in the subsequent circuit stage and a tracking algorithm sufficiently fast related to environmental changes, the transducer behavior can be further simplified to its specific open-circuit voltage and output power curves. This information can be extracted from transducer datasheets or application-specific in controlled lab experiments. The exemplary behavior of a solar cell for different lighting and load conditions is visualized in Fig. 3 (a). The magenta marked curve in the
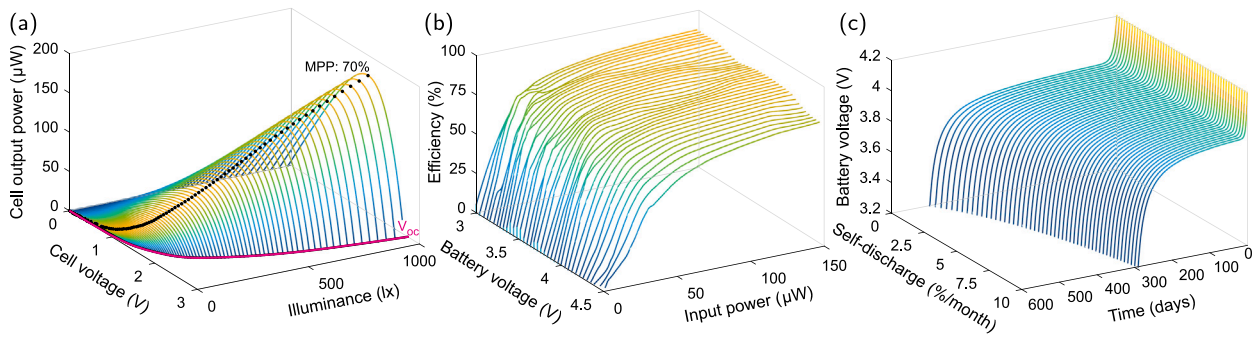
Fig. 3. Visualization of the individual simulation model blocks. (a) Solar cell output power as a function of the MPP configuration and the illuminance. The open-circuit voltage of the transducer is marked (magenta) in the 0 W plane. The corresponding MPPs are highlighted in black at 70 % of V_{OC}. (b) The conversion efficiency of the EH boost converter as a function of the input power and the battery voltage. (c) Extended Li-Ion battery model with self-discharge characteristics.

Table 3
Validation results for the converter efficiency regression model.

Metric	Definition		Result
MAE	$\frac{1}{n}\sum_{i=1}^{n}\lvert \hat{\eta}_i - \eta_i \rvert$	(1)	0.42 %
$RMSE$	$\sqrt{\frac{1}{n}\sum_{i=1}^{n}\left(\hat{\eta}_i - \eta_i\right)^2}$	(2)	0.75 %
R^2	$1 - \frac{\sum_{i=1}^{n}\left(\hat{\eta}_i - \eta_i\right)^2}{\sum_{i=1}^{n}\left(\eta_i - \frac{1}{n}\sum_{j=1}^{n}\eta_j\right)^2}$	(3)	1.00

0 W plane illustrates the cell's open-circuit voltage V_{OC} as a function of the illuminance. The corresponding peak output power, measured cell-specific at 70 % of the open-circuit voltage, is marked with black dots. Both curves can be approximated piece-wise with higher-order polynomials.

4.2. Energy harvesting circuit model

Essential for any self-sustaining EH-powered sensor node is the energy management circuitry, which acts as an interface between the circuit and EH transducer and provides basic sequence control and storage element protection [3]. State-of-the-art commercial integrated energy harvesting circuits are feature-rich and only partly disclosed, making an accurate model design complex or often even impossible. This limitation can be circumvented to a certain extent by analysis of the circuit behavior based on exhaustive measurements combined with statistical modeling. A constraint for such a data-driven model creation is the characterization time, which increases exponentially with the model's degrees of freedom. A priori knowledge of the targeted EH transducer, and with that, a defined input current–voltage characteristic and maximal power point (MPP) setting, allows shortening the characterization time significantly, however, at the cost of substitutability.

In the context of this work, the energy harvesting and power management circuit presented in [40], which is based on the popular TEXAS INSTRUMENTS BQ25570 energy harvesting converter, has been analyzed and modeled to provide an exemplary practical illustration of the model building methodology. The harvesting circuit was tested over wide operational conditions to characterize the circuit's energy conversion efficiency by replacing the EH transducer and storage element with a programmable source measurement unit. In addition, the integrated MPPT circuitry, with a sampling interval of 16 s, has been bypassed with an external source to accelerate the characterization. This allows determining circuit behavior as a function of input voltage, input current, storage element voltage, and MPPT configuration. The high number of input parameters results in over 10^7 data points with a measurement time of more than a week. Subsequently, a Gaussian process regression

model was trained to determine the circuit efficiency as a function of the circuit state. The trained model can be afterward compiled as a MATLAB SIMULINK executable function. Table 3 summarizes the 5-fold cross-validation results of the regression model. Under the assumption of matched operation, the efficiency model shows a mean absolute error (MAE) of 0.42 %, a root mean square error (RMSE) of 0.75 %, and a determination coefficient (R^2) of 1.00. Other characteristics, such as idle consumption and overcharge protection, have been considered with conditional statements. An exemplary part of the model is shown in Fig. 3(b), visualizing the circuit's efficiency drop for low input power and increased DC–DC boost converter ratio.

4.3. Energy storage element model

The energy storage element chemistry and capacity define energy density and peak discharge current. Thus, the storage element is crucial for decoupling source and load power points and, with it, the applicability of the system design. Storage element dynamics are broadly analyzed in the literature, allowing the utilization of existing models [30–32,41–43]. These models consider cell chemistry and cell topology in addition to advanced characteristics such as aging and temperature effects.

Li-Ion Battery — The Li-Ion charge and discharge behavior can be approximated as a controlled non-linear and non-ideal voltage source as presented in [30]. The model considers polarization effects according to Eq. (4).

$$
\begin{aligned}
V_{bat} =\ & E_0 - Ri + Ae^{-B\,it} \\
& - \underbrace{K\frac{Q}{Q-it}i^*}_{\substack{Polarization \\ Resistance}} - \underbrace{K\frac{Q}{Q-it}it}_{\substack{Polarization \\ Voltage}} - \underbrace{R\,D\frac{it}{Q}}_{\substack{Self-discharge \\ Voltage}}
\end{aligned} \tag{4}
$$

where:

V_{bat}	battery voltage	[V]
E_0	battery constant voltage	[V]
K	polarization constant	[Ω]
Q	battery capacity	[A h]
it	$\int i\,dt$ = actual battery charge	[A h]
A	exponential zone amplitude	[V]
B	exponential zone constant	[1/(A h)]
D	self-discharge constant	[A]
R	internal resistance	[Ω]
i	battery current	[A]
i^*	filtered current	[A]

The charge and discharge characteristics are considered with alternating polarization resistances. During charging, the polarization resistance can be approximated as $K\frac{Q}{it-0.1Q}$. The original model presented in [30] has been extended with simplified self-discharge characteristics

to consider longtime effects, which are critical for EH-powered sensor nodes. Li-Ion typically, the self-discharge current has been described as a percentage of the state-of-charge per month. The model output for a 12 mA h single-cell Li-Ion battery with a constant 1 μA load and variable self-discharge rates is visualized in Fig. 3(c).

Supercapacitor — In contrast to more complex battery chemistries, capacitors in light load operation can be approximated with the non-ideal capacitor equivalent circuit. In the simplified circuit, the highly relevant self-discharge characteristics are directly accounted for by the parallel leakage resistance. A better approximation, especially for a capacitor size of several F, is achieved by an RC ladder circuit with voltage-dependent capacity as introduced in [32] or with the Gouy–Chapman–Stern model [42].

4.4. Load model

The limited harvested energy of small-sized EH transducers inevitably results in the need to balance the available with the consumed energy. Among other techniques, Duty Cycling (DC), i.e., switching-off major parts of the sensor nodes for a predetermined period to save energy and activate the full system only for a short interval, demonstrated effectiveness in matching the power input with the consumed energy. A more recent trend is the dynamic adaption of the load energy consumption based on extrinsic information. In such an event-driven scenario, either an always-on wake-up circuitry detects events of interest to activate the full system, or the available energy itself is used as a trigger with so-called transient or intermittent computing [20,21,44].

The sensor load profile is highly application-specific and requires manual characterization to simulate the full system. For duty-cycled operation, the load can be described based on apriori knowledge of the system's idle consumption and the energy required for a single system activation. Under the assumption of a duty-cycle T significantly larger than the active time T_{on}, which is valid for deep-duty cycled operation, the load can be approximated as described in Eq. (5).

$$P_{LOAD}(t, V_{bat}) = P_{IDLE}(V_{bat}) + \frac{E_{ON}(V_{bat})}{T_{ON}} \sum_{n=1}^{\infty} \mathcal{H}(t - nT + T_{ON}) - \mathcal{H}(t - nT) \quad (5)$$

Depending on the storage element chemistry and voltage conversion strategy, the storage voltage can significantly influence the load consumption. Thus, the idle consumption P_{IDLE} and periodical load E_{ON} should be modeled as a function of the storage element voltage V_{bat}.

4.5. Complete sensor node model

The description of the individual circuit blocks and their dynamic behavior allows the assembly of a complete sensor node model focused on power transfer, as shown in Fig. 2. As an input variable, the model requires an application-specific ambient energy dataset, represented by a time series of the harvester's intrinsic physical measurand, e.g., illuminance, temperature gradient, acceleration, field strength, etc. The EH transducer model subsequently converts the environmental data into power and voltage signals, thus allowing the parametrization or substitution of the EH transducer without recollecting ambient data. The harvesting circuit model further conditions the transducer output power under consideration of input and battery voltage. In addition to this dynamic harvesting efficiency, storage element over- and undervoltage protection and MPP configuration are programmed statically. The harvesting circuit is connected bidirectionally to the battery model allowing a negative charge power in case of energy dry periods. Finally, the voltage dependent load model is connected in parallel to the battery.

The combined model implemented in MATLAB SIMULINK V10.5 (R2022a) using an ode23t solver in accelerator mode reaches 10^4 obs/s

Table 4
Specifications of the exemplary EH powered sensing node.

	Description
EH dataset	[34], #06 — office space with little natural light illuminance (day) 112 ± 52 lx, ~2 year data
EH transducer	ANYSOLAR KXOB25-02X8F 23 × 8 × 1.8 mm, 0.6 g
EH circuit	[40], TI BQ25570 MPPT 70 %, overcharge protection 4.2 V
Energy storage element	(A) LiPo, 12 mA h, 12 × 8 × 3 mm, 0.35 g (B) Capacitor, FC0H104ZFT, 100 mF, 1.0 g
Load profile	NORDIC nRF52832 BLE IC advertising (TX only), payload 30 byte

running on a laptop computer (i7-6850U). Thus a one-year-long dataset sampled at 1/60 Hz results in a simulation time of approximately 1 min.

The block-based design allows high flexibility and adaptability of the proposed system model. This could include, for instance, a more precise description of individual control algorithms such as the MPPT tracking or cold-start behavior. Beyond that, topology modifications are possible without great effort, e.g., convert-less power paths or multi-source harvesters.

5. Experimental results

An exemplary sensor node introduced in Section 5.1 is analyzed to evaluate the accuracy of the proposed model-based design approach and the applicability in the development process of self-sustainable sensor nodes. First, in Section 5.2, the model is parameterized and verified in terms of simulation accuracy. Subsequently, in 5.3, the self-sustainability of the parameterized virtual prototype is analyzed over a two-year simulated time span, and the outcome is compared to state-of-practice methods. Finally, in 5.4 and 5.5, design decisions are validated, and optimization potential for the sensor node is identified.

5.1. Exemplary autonomous wireless sensor node

To demonstrate the advantages and limitations of the proposed model-based design approach, an exemplary small-sized solar-powered sensor node, summarized in Table 4, has been analyzed. The system is powered by an ANYSOLAR KXOB25-02X8F mono-crystalline solar cell connected to a BQ25570 energy harvesting circuit. A 12 mA h large single cell LiPo battery and a 100 mF supercapacitor are selected to analyze the impact of the storage element selection. As a load, a NORDIC nRF52832 Bluetooth low energy (BLE) system-on-chip in advertising configuration is considered. The payload is assumed to be 30 byte resulting in a typical energy per advertising event of 37 μJ, including 10 % conversion losses. The system is assumed to be deployed in a low-light office environment based on the illuminance from the dataset presented in [34] collected at sensor position #06.

5.2. Model verification

To verify the created model, the physical prototype is analyzed under controllable and repeatable environmental conditions. This is achieved by placing the solar cell in a darkened chamber, artificially illuminated by a controllable broadband light source. Thus, the circuit behavior can be precisely monitored while emulating realistic indoor light scenes. In particular, the following experimental setup has been used to determine unknown battery parameters and assess the simulation model's performance:

The illuminance is controlled and monitored with two software-controlled source/measurement units (SMU), KEYSIGHT N6782A, connected to a halogen lamp and a photoresistor. Currents and voltages are logged with KEYSIGHT 34465A multimeters in high-z input configuration between solar cell and energy harvesting converter as well as between
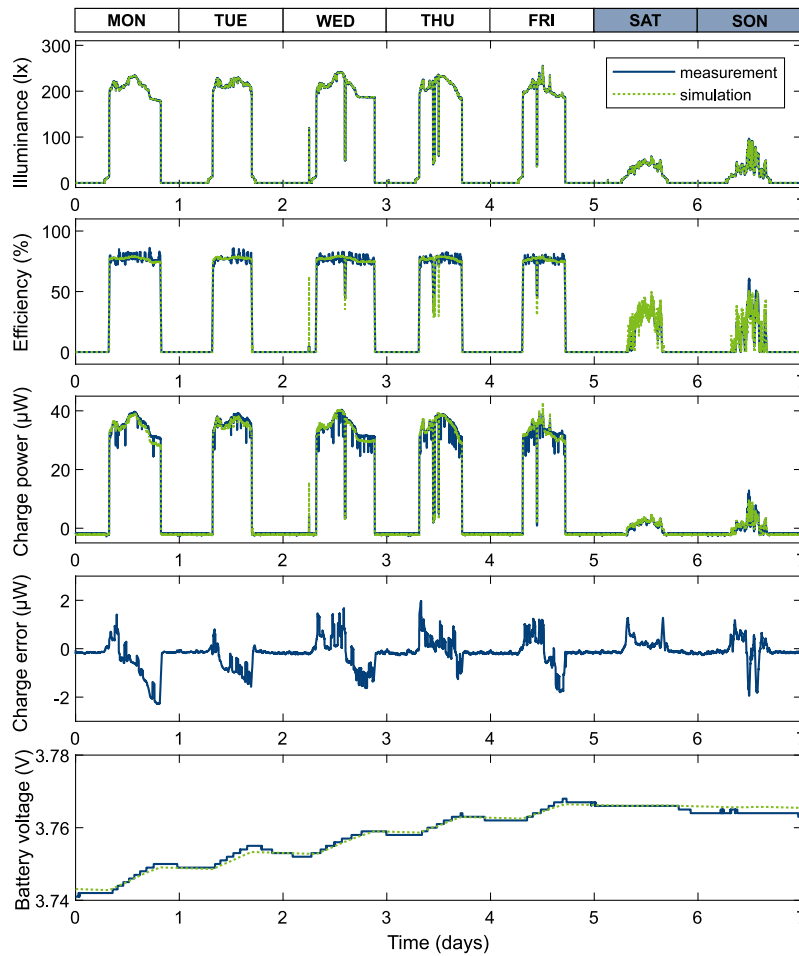
Fig. 4. Model verification based on a one-week-long measurement under controlled lab conditions. Simulation and measurement consider a LiPo battery with a nominal capacity of $12\,\text{mA}\,\text{h}$ as an energy storage element.

converter and battery. Finally, the load is emulated with a highly precise KEYSIGHT B2902A SMU connected parallel to the battery. All measurements are conducted at a constant room temperature of $25\,°\text{C}$.

Fig. 4 shows the model verification results based on a one-week-long controlled lab experiment. To compensate for errors caused by the degeneration of the lamp during longtime data acquisition, the measured illuminance is used as an input source for the simulation model. In addition to the illumination, the battery capacity, which comprises considerable tolerances due to process variation and aging, is determined from the cell voltage change in known charging conditions. The first subplot of Fig. 4 illustrates the illuminance in lux emulating a low-light office scene with a relatively stable illumination of $200\,\text{lx}$ during working time and reduced light below $100\,\text{lx}$ during the weekend. The second subplot shows the conversion efficiency of the EH boost converter. A typical $1.73\,\text{V}$ solar cell open-circuit voltage and the resulting favorable boost conversion ratio allow a harvesting efficiency of up to $86\,\%$ during working hours. In contrast, the limited illumination on the weekend causes a drop in input voltage and power, reducing the EH boost converter efficiency below $50\,\%$. Subplots three and four show the battery charge power and the corresponding error expressed in μW between measurement and simulation. During the night, or more precisely, for an illuminance below $10\,\text{lx}$, the system operates solely from the energy stored in the battery visualized by a negative charge current. The error shown in subplot four is visualized as a mean calculated of a sliding window with a length of $15\,\text{min}$. Finally, the lowest subplot illustrates the battery voltage in the analyzed period.

The model performance metrics resulting from the verification experiment are summarized in Table 5, where $\hat{P}_{CH}$ represents the predicted battery charge power of the model and P_{CH} the measured

counterpart. The results show a root mean square error of $1.47\,\mu\text{W}$ for the power balance between measurement and simulation in the $7\,\text{d}$ long period. Normalized by the mean measured charge power, this results in an $nRMSE$ of 0.146. The model's coefficient of determination can be calculated according to as 0.992.

By integrating the measured and simulated battery charge power over time, the energy error ($E_{error\,\%}$) can be calculated following as $-1.57\,\%$ in the analyzed timeframe. In a similar manner, the mean daily energy error ($\overline{E}_{24h\,error}$) can be calculated as $13.7\,\text{mJ/d}$. The precise replication of the circuit dynamics demonstrates simulation accuracy with a negligible error compared to component tolerances.

5.3. Longtime analysis

In the state-of-practice approach, with static circuit parameters and known environmental conditions, the harvested power P_{EH} can be approximately calculated based on the expected illuminance E_V, the cell output power in matched conditions P_{MPP}, and the estimated boost converter efficiency η, Eq. (12).

$$P_{EH}(t) = E_V(t) \frac{P_{MPP\,@\,1\,\text{W/m}^2}}{\alpha} \eta \qquad (12)$$

The parameter $\alpha \approx 120\,\text{lx}$ allows converting the cell output power from power-per-irradiance to power-per-illuminance [45]. Applied on the duty-cycled EH-powered sensor, the battery state-of-charge (SoC) can be calculated by integrating the power balance over time, Eq. (13).

$$SoC(t) = SoC(0) + \frac{1}{QV_{nom}} \int_0^t P_{EH}(t) - P_{PM} - \frac{E_{ADV}}{T_{ADV}} - P_{SD}\ dt \qquad (13)$$

Table 5
Model verification results.

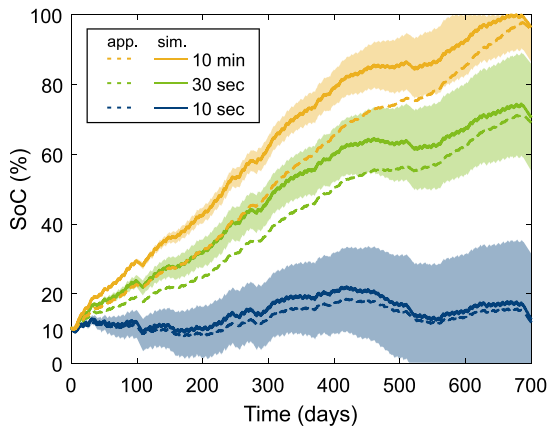| Metric	Definition		Result
MAE	$\frac{1}{n}\sum_{i=1}^{n}\left|\hat{P}_{CH,i} - P_{CH,i}\right|$	(6)	0.56 μW
$RMSE$	$\sqrt{\frac{1}{n}\sum_{i=1}^{n}\left(\hat{P}_{CH,i} - P_{CH,i}\right)^2}$	(7)	1.47 μW
$nRMSE$	$\dfrac{RMSE}{\frac{1}{n}\sum_{i=1}^{n}P_{CH,i}}$	(8)	0.146
R^2	$1 - \dfrac{\sum_{i=1}^{n}\left(\hat{P}_{CH,i} - P_{CH,i}\right)^2}{\sum_{i=1}^{n}\left(P_{CH,i} - \frac{1}{n}\sum_{j=1}^{n}P_{CH,j}\right)^2}$	(9)	0.992
$E_{error\,\%}$	$\dfrac{\int \hat{P}_{CH,i}(t)\,dt}{\int P_{CH,i}(t)\,dt} - 1$	(10)	−1.57 %
$\overline{E}_{24h\,error}$	$\frac{1}{n}\sum_{i=1}^{n}\int^{24h}\hat{P}_{CH,i}(t) - P_{CH,i}(t)\,dt$	(11)	−13.7 mJ/d

Fig. 5. Longtime simulation of the exemplary wireless sensor node for three advertising intervals. The shaded areas visualize the uncertainty due to component tolerances. The approximated SoC based on a state-of-practice calculation with static parameters is illustrated as dashed lines.

Where Q is the battery capacity in ampere-seconds and V_{nom} is the nominal battery voltage. The power balance considers next to the harvested power P_{EH}, the static consumption of the power management P_{PM}, the power consumption during advertising as energy per advertising event E_{ADV} divided by the advertising duration T_{ADV}, and the typical battery self-discharge power P_{SD}.

A comparison between the simulation and the approximated calculation is given in Fig. 5. The analysis is based on two years of illuminance data and shows the estimated SoC for an advertising interval of 10 s, 30 s, and 10 min. To visualize the influence of component tolerances, shown as shaded areas, the circuit variability is considered with an MPPT and over-charger protection (OCP) programming accuracy of ±1 %, a cell output power variation of ±10 %, and a battery capacity tolerance of ±20 %. The comparison of the simulation (including component tolerance) to the approximated calculation, drawn as dashed lines, shows a SoC mismatch of up to 10 %, respectively 13.04 W s. The result suggests that the approximation provides good results for a system operation close to the energy neutrality ($T_{ADV} = 10$ s). This is due to the relatively constant battery voltage. In contrast to that, a more conservative and thus energy-positive operation results in a significant error during the charging period. System tolerances, and subsequently a deviation of the harvested power, accumulate over time until the system reaches an equilibrium due to the OCP at a fully charged battery. Considering tolerances is particularly vital if an operation close to energy-neutrality is targeted, e.q. in the analyzed light situation, a long-term operation cannot be guaranteed for a 10 s advertising interval. The depicted example also shows the importance

of a longtime analysis. Despite the seasonal fluctuations of the harvested power, the state-of-charge (SoC) in the worst-case scenario implicates an energy-neutral operation in the first year. In the second year, the same configuration would clearly run into an under-voltage lockout ($SoC = 0\%$) due to a small reduction of the environmental energy.

5.4. System optimization

In addition to the long-term analysis of self-sustainability, the parameterizable model also allows the validation of individual design decisions alongside the optimization of system parameters. Fig. 6 visualizes such exemplary parameter sweeps by consecutively varying battery capacity, battery self-discharge, and BLE advertising interval. The resulting impact on the system's energy storage usage is shown as a mean of the state-of-charge in the analyzed two-year-long observation period. The variations due to component tolerances are shown as shaded areas.

A variation of the battery capacity with a constant advertising period suggests reducing the battery capacity to 1 mA h, Fig. 6(a). This capacity would be sufficient to balance energy fluctuations while lowering system cost and size. Alongside the battery capacity reduction, losses due to self-discharge would be reduced at the cost of a smaller energy buffer in energy dry periods. The battery's peak discharge current rating is a crucial criterion limiting such a substantial reduction. For instance, the exemplary sensor node introduced in Section 5.1, with its NORDIC nRF52832 BLE IC, requires a peak current of up to 9 mA during transmission. This results, under the assumption of a battery with a discharge rate of 1 C, in a needed capacity of at least 9 mA h, significantly higher than the optimum of Fig. 6(a).

The storage element self-discharge can considerably influence the energy balance of an EH-powered system. Fig. 6(b) visualizes the impact of a varying self-discharge rate on the average SoC for constant battery size and advertising interval. A large battery self-discharge rate results in a slower battery charging and, for the analyzed scenario, in a worse utilization of the battery capacity. In the analyzed scenario, the 12 mA h sized battery shows a negligible influence on the energy balance for self-discharge rates below 4 %/month.

Fig. 6(c) illustrates the influence of the BLE advertising interval on the energy balance. For advertising intervals above 100 s, the contribution of the load on the overall energy balance is negligible. Below 100 s advertising intervals, the impact of the load gets dominant, and the system approaches rapidly to the limit of energy neutrality, defined as the initial battery charge ($SoC = 10\%$). The limit for self-sustainable operation under consideration of the tolerances is a BLE advertising every 12 s.

For the exemplary sensor node analyzed, the quality of service could be defined as a function of the BLE advertising interval (responsiveness) and resilience against energy dry periods (availability). Fig. 7 shows this trade-off under consideration of a varying storage element capacity. The dark-blue area defines the configurations that do not allow perpetual operation due to insufficient storage capacity (< 1 mA h) or too short advertising intervals (< 12 s). In contrast, the yellow area of Fig. 7 visualizes configurations that allow accumulating sufficient energy to operate over one week without energy harvesting, however, at the cost of unnecessary high advertising intervals (> 100 s). A favorable configuration that balances advertising interval and battery size without significantly compromising on the resilience against energy dry periods lays between these extremes at a battery capacity of 7 mA h and an advertising interval of 90 s.
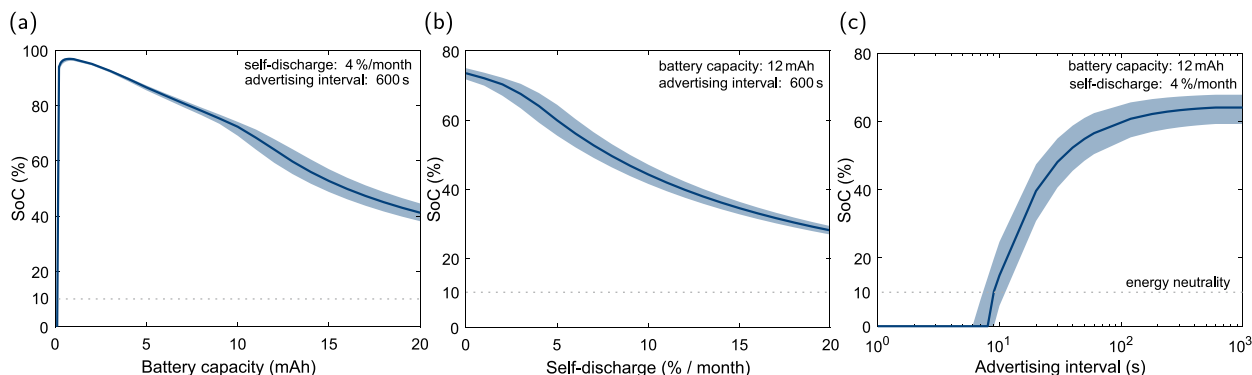
Fig. 6. System analysis based on parameter sweeps. (a) Impact of the battery capacity on the mean state-of-charge. (b) Battery self-discharge rate as a significant contributor to the overall energy balance. (c) Optimal selection of the BLE advertising interval to match harvested with consumed energy.
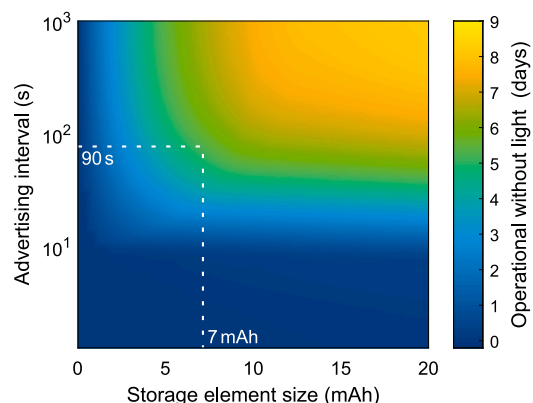

Fig. 7. Optimal system parametrization under consideration of availability and responsiveness.

5.5. Storage element chemistry selection

The findings in Section 5.4, which demonstrate stable system operation despite small storage element capacity, suggest replacing the LiPo battery with a supercapacitor. However, this modification can significantly influence the sensor node dynamic behavior. The temporal closer coupling between the source and load power points and the capacitor charge curve results in a substantially higher storage element voltage variation. Alongside this variation, which depends on the programmed maximal capacitor voltage and influences the end-to-end conversion efficiency, the leakage current typically rises for capacitors compared to small-sized batteries [19]. Fig. 8 shows the model verification with a 100 mF KEMET FC0H104ZFT supercapacitor as an energy storage element. Except for the capacitor, a similar evaluation setup and illuminance data described in Section 5.2 are used. The overcharge protection has been programmed to 4.5 V to account for the wider storage voltage range.

The system behavior can be simulated accurately after determining the actual capacity and self-discharge rate from the verification measurement. In contrast to the LiPo-based circuit, the overcharge protection is triggered repeatedly, resulting in poor utilization of the available energy. In addition, the 100 mF capacity is insufficient to ensure stable operation on the energy dry weekend.

The comparison between measurement and simulation also reveals the limits of the model. Triggering the overcharge protection due to reaching the programmed maximal storage element voltage of 4.5 V results in a repeated deactivation of the harvesting circuitry. The circuit behavior during this alternating mode of operation is only considered statically in the model and ignores transient switching and the

corresponding losses shown in subfigure 3 of Fig. 8. In addition, the hardware programmed overcharge protection varies due to component tolerances. This results in a short-term mismatch between model and simulations and an increased charge error at the beginning of every over-charge protection phase, visible in subfigure 4 of Fig. 8. It is important to notice that the temporary mismatch during over-charge protection periods has no influence on the long-term performance of the model as the storage element voltage and the stored energy is predicted correctly. Finally, the model shows an increased charge error during the under-voltage lockout. For battery voltages below 3.0 V, the circuit operates outside the parameter space used for training the harvesting circuit regression model. Thus, the model is not able to correctly predict the circuit efficiency outside the intended operating range.

Independently of the mentioned corner case, the accurate and parameterizable model allows the search for an application-specific optimal capacitor size. Fig. 9 visualizes this search by sweeping capacitor size and self-discharge rate. The axes show the capacitor size and the self-discharge rate normalized by the capacitor size. The colors illustrate the time until the simulation predicts the first under-voltage lockout event. The results suggest that no capacitor with a similar capacitance to self-discharge ratio would allow a self-sustainable operation in the targeted application scenario. In fact, a 2 to 3 times lower self-discharge rate, illustrated as a yellow area, would be required to outlast the 700 day long simulation without an under-voltage lockout. This demonstrates the importance of the storage element selection in the design of EH-powered devices and the potential of the model-based design. The accurate model allows a reliable and rapid analysis of the system behavior over various configurations together with the early identification of design errors.

6. Conclusion

This work presented a model-based design approach in the context of self-sustainable sensors. The model has been assessed in comparison with actual hardware. This includes the derivation and discussion of simulation models for the key building blocks of energy-efficient systems powered by energy harvesting and the verification of the models based on comprehensive lab experiments. Finally, the virtual prototype was used to identify optimization potential and validate design decisions.

An exemplary emulation of a solar-powered wireless sensor node demonstrated the advantages of the proposed approach. The model verification showed a coefficient of determination (R^2) of 0.992 for the power balance between measurement and simulation, proofing the viability of data-driven modeling of state-of-the-art EH boost converters. With an energy error of -1.57%, longtime energy neutrality can be assessed accurately and reliably. A comparison to state-of-practice analytical modeling showed an SoC deviation of up to 10 % despite considering generous component tolerances in the presented approach.
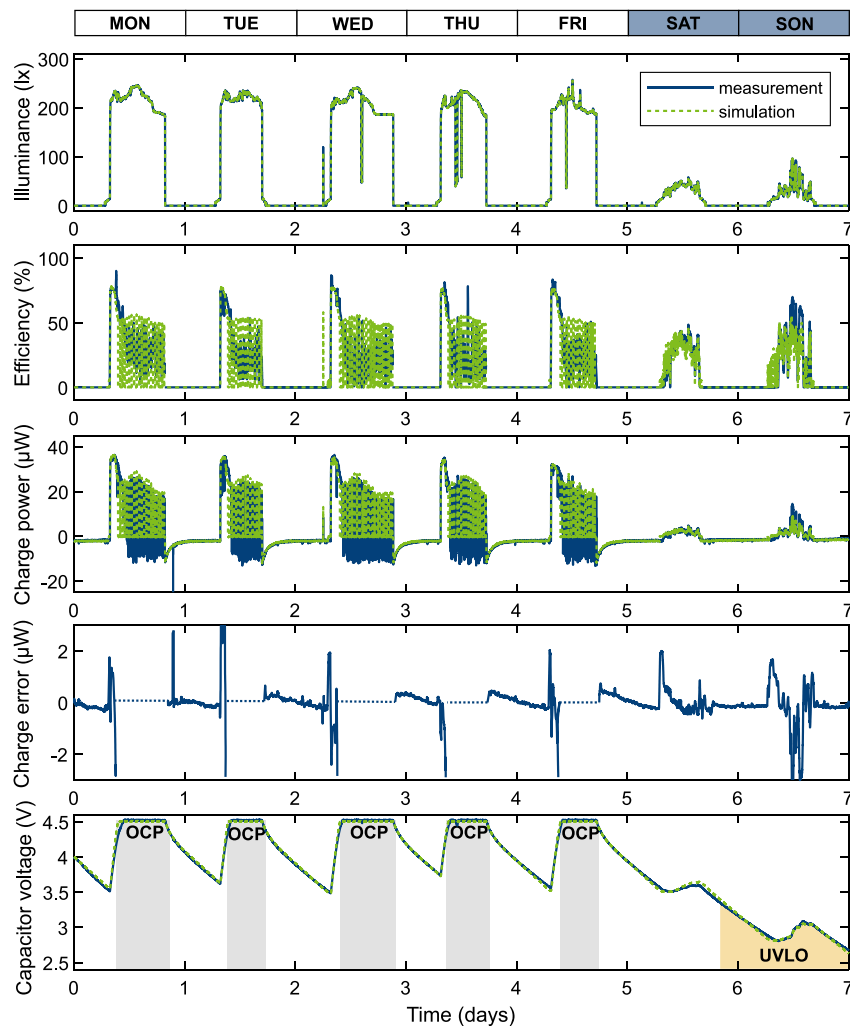
Fig. 8. Model verification based on a one-week-long measurement under controlled lab conditions. Simulation and measurement consider a supercapacitor with a nominal capacity of 100 mF as an energy storage element.
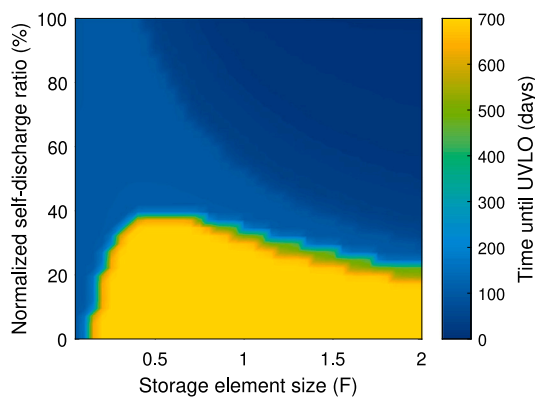

Fig. 9. Supercapacitor requirements to enable self-sustainable operation. SoA capacitors suffer from a 2 to 3 times too high self-discharge rate to enable the exemplary application scenario.

Supported by the flexibility and configurability of the virtual prototype, an application-specific balance between sensor advertising and storage element size has been determined. During the analysis, the limitations of today's energy storage elements for compact and energy-efficient sensor nodes were analyzed. The low average consumption due to deep-duty cycled operation combined with the battery capacity depended on the self-discharge rate favors small-sized batteries. This results typically in a peak current bound battery selection. In contrast, today's supercapacitors' capacity to self-discharge ratio significantly limits their usability when combined with state-of-the-art sub-μW circuits.

In conclusion, the paper demonstrated the accurate modeling of the energy balance of EH-powered sensor nodes, which lays the foundation for a much wider analysis, spanning from the validation of energy harvesting and management circuits to the design and test of energy predictive algorithms in realistic longtime conditions.

CRediT authorship contribution statement

Philipp Mayer: Conceptualization, Methodology, Software, Hardware, Investigation, Writing – original draft. **Michele Magno:** Conceptualization, Validation, Writing – review & editing. **Luca Benini:** Supervision, Writing – review & editing.

Declaration of competing interest

The authors declare that they have no known competing financial interests or personal relationships that could have appeared to influence the work reported in this paper.

Data availability

Data will be made available on request.

References

[1] Aazam M, Zeadally S, Harras KA. Deploying fog computing in industrial Internet of Things and industry 4.0. IEEE Trans Ind Inf 2018;14(10):4674–82. http://dx.doi.org/10.1109/TII.2018.2855198.

[2] Compare M, Baraldi P, Zio E. Challenges to IoT-enabled predictive maintenance for industry 4.0. IEEE Internet Things J 2020;7(5):4585–97. http://dx.doi.org/10.1109/JIOT.2019.2957029.

[3] Newell D, Duffy M. Review of power conversion and energy management for low-power, low-voltage energy harvesting powered wireless sensors. IEEE Trans Power Electron 2019;34(10):9794–805. http://dx.doi.org/10.1109/TPEL.2019.2894465.

[4] Ma D, Lan G, Hassan M, Hu W, Das SK. Sensing, computing, and communications for energy harvesting IoTs: A survey. IEEE Commun Surv Tutor 2020;22(2):1222–50. http://dx.doi.org/10.1109/COMST.2019.2962526.

[5] Magno M, Boyle D. Wearable energy harvesting: From body to battery. In: 2017 12th international conference on design technology of integrated systems in nanoscale era. 2017, p. 1–6. http://dx.doi.org/10.1109/DTIS.2017.7930169.

[6] Sherazi HHR, Grieco LA, Imran MA, Boggia G. Energy-efficient LoRaWAN for industry 4.0 applications. IEEE Trans Ind Inf 2021;17(2):891–902. http://dx.doi.org/10.1109/TII.2020.2984549.

[7] Liebel G, Marko N, Tichy M, Leitner A, Hansson J. Model-based engineering in the embedded systems domain: An industrial survey on the state-of-practice. Softw Syst Model 2018;17(1):91–113. http://dx.doi.org/10.1007/s10270-016-0523-3.

[8] Li L, Soskin NL, Jbara A, Karpel M, Dori D. Model-based systems engineering for aircraft design with dynamic landing constraints using object-process methodology. IEEE Access 2019;7:61494–511. http://dx.doi.org/10.1109/ACCESS.2019.2915917.

[9] Younse PJ, Cameron JE, Bradley TH. Comparative analysis of model-based and traditional systems engineering approaches for architecting a robotic space system through automatic information transfer. IEEE Access 2021;9:107476–92. http://dx.doi.org/10.1109/ACCESS.2021.3096468.

[10] Jensen JC, Chang DH, Lee EA. A model-based design methodology for cyber-physical systems. In: 2011 7th international wireless communications and mobile computing conference. 2011, p. 1666–71. http://dx.doi.org/10.1109/IWCMC.2011.5982785.

[11] Molina JM, Damm M, Haase J, Holleis E, Grimm C. Models, methods, and tools for complex chip design. Springer International Publishing; 2014, p. 127–43.

[12] Hadas Z, Janak L, Smilek J. Virtual prototypes of energy harvesting systems for industrial applications. Mech Syst Signal Process 2018;110:152–64. http://dx.doi.org/10.1016/j.ymssp.2018.03.036.

[13] San Miguel J, Ganesan K, Badr M, Jerger NE. The EH model: Analytical exploration of energy-harvesting architectures. IEEE Comput Archit Lett 2018;17(1):76–9. http://dx.doi.org/10.1109/LCA.2017.2777834.

[14] Vasilevski M, Queiroz E, Fonseca AL, Silva I, Catunda SY, Guedes LA. SystemC AMS modeling of a sensor node energy consumption and battery state-of-charge for WSN. In: 2015 IEEE 13th international new circuits and systems conference. 2015, p. 1–4. http://dx.doi.org/10.1109/NEWCAS.2015.7181996.

[15] Heller J, Niemann C, Plockstsies F, Haubelt C, Timmermann D. Towards virtual prototyping of electrically active implants using SystemC-AMS. In: MBMV 2020 — Methods and description languages for modelling and verification of circuits and systems; GMM/ITG/GI-workshop. 2020, p. 1–8.

[16] Yue X, Kauer M, Bellanger M, Beard O, Brownlow M, Gibson D, et al. Development of an indoor photovoltaic energy harvesting module for autonomous sensors in building air quality applications. IEEE Internet Things J 2017;4(6):2092–103. http://dx.doi.org/10.1109/JIOT.2017.2754981.

[17] Thielen M, Sigrist L, Magno M, Hierold C, Benini L. Human body heat for powering wearable devices: From thermal energy to application. Energy Convers Manage 2017;131:44–54. http://dx.doi.org/10.1016/j.enconman.2016.11.005.

[18] Adu-Manu KS, Adam N, Tapparello C, Ayatollahi H, Heinzelman W. Energy-harvesting wireless sensor networks (EH-WSNs): A review. ACM Trans Sen Netw 2018;14(2). http://dx.doi.org/10.1145/3183338.

[19] Jackson N, Adkins J, Dutta P. Reconsidering batteries in energy harvesting sensing. In: Proceedings of the 6th international workshop on energy harvesting & energy-neutral sensing systems. New York, NY, USA: Association for Computing Machinery; 2018, p. 14–8. http://dx.doi.org/10.1145/3279755.3279757.

[20] Merrett GV, Al-Hashimi BM. Energy-driven computing: Rethinking the design of energy harvesting systems. In: Design, automation test in Europe conference exhibition. 2017, p. 960–5. http://dx.doi.org/10.23919/DATE.2017.7927130.

[21] Lin L, Jain S, Alioto M. Integrated power management for battery-indifferent systems with ultra-wide adaptation down to nW. IEEE J Solid-State Circuits 2020;55(4):967–76. http://dx.doi.org/10.1109/JSSC.2019.2959742.

[22] Abuellil A, Estrada-López JJ, Bommireddipalli A, Costilla-Reyes A, Zeng Z, Sánchez-Sinencio E. Multiple-input harvesting power management unit with enhanced boosting scheme for IoT applications. IEEE Trans Ind Electron 2020;67(5):3662–72. http://dx.doi.org/10.1109/TIE.2019.2920607.

[23] Mayer P, Magno M, Benini L. Energy-positive activity recognition — from kinetic energy harvesting to smart self-sustainable wearable devices. IEEE Trans Biomed Circuits Syst 2021;15(5):926–37. http://dx.doi.org/10.1109/TBCAS.2021.3115178.

[24] Götz M, Kanoun O. Ultralow power voltage supervisor for ambient power-driven microcontroller systems. IEEE Trans Ind Electron 2019;66(5):3843–51. http://dx.doi.org/10.1109/TIE.2018.2851981.

[25] Sigrist L, Gomez A, Leubin M, Beutel J, Thiele L. Environment and application testbed for low-power energy harvesting system design. IEEE Trans Ind Electron 2021;68(11):11146–56. http://dx.doi.org/10.1109/TIE.2020.3036222.

[26] Xue T, Williams S, Rantz R, Halim MA, Roundy S. System modeling, characterization, and design considerations for generators in commercial watches with application to energy harvesting for wearables. IEEE/ASME Trans Mechatronics 2018;23(5):2515–24. http://dx.doi.org/10.1109/TMECH.2018.2865307.

[27] Vostrikov S, Somov A, Gotovtsev P, Magno M. Comprehensive modelling framework for a low temperature gradient thermoelectric generator. Energy Convers Manage 2021;247:114721. http://dx.doi.org/10.1016/j.enconman.2021.114721.

[28] Yi Z, Yang B, Zhang W, Wu Y, Liu J. Batteryless tire pressure real-time monitoring system driven by an ultralow frequency piezoelectric rotational energy harvester. IEEE Trans Ind Electron 2021;68(4):3192–201. http://dx.doi.org/10.1109/TIE.2020.2978727.

[29] Hasani M, Irani Rahaghi M. The optimization of an electromagnetic vibration energy harvester based on developed electromagnetic damping models. Energy Convers Manage 2022;254:115271. http://dx.doi.org/10.1016/j.enconman.2022.115271.

[30] Tremblay O, Dessaint L-A. Experimental validation of a battery dynamic model for EV applications. World Electr Veh J 2009;3(2):289–98. http://dx.doi.org/10.3390/wevj3020289.

[31] Tremblay O, Dessaint L-A, Dekkiche A-I. A generic battery model for the dynamic simulation of hybrid electric vehicles. In: 2007 IEEE vehicle power and propulsion conference. 2007, p. 284–9. http://dx.doi.org/10.1109/VPPC.2007.4544139.

[32] Weddell AS, Merrett GV, Kazmierski TJ, Al-Hashimi BM. Accurate supercapacitor modeling for energy harvesting wireless sensor nodes. IEEE Trans Circuits Syst II: Express Briefs 2011;58(12):911–5. http://dx.doi.org/10.1109/TCSII.2011.2172712.

[33] Li X, Zhang X, Lin F, Blaabjerg F. Artificial-intelligence-based design (AI-D) for circuit parameters of power converters. IEEE Trans Ind Electron 2021;1. http://dx.doi.org/10.1109/TIE.2021.3088377.

[34] Sigrist L, Gomez A, Thiele L. Dataset: Tracing indoor solar harvesting. In: Proceedings of the 2nd workshop on data acquisition to analysis. New York, NY, USA: Association for Computing Machinery; 2019, p. 47–50. http://dx.doi.org/10.1145/3359427.3361910.

[35] Gorlatova M, Wallwater A, Zussman G. Networking low-power energy harvesting devices: Measurements and algorithms. In: 2011 proceedings IEEE INFOCOM. 2011, p. 1602–10. http://dx.doi.org/10.1109/INFCOM.2011.5934952.

[36] Sobral VAL, Lach J, Goodall JL, Campbell B. Thermal energy harvesting profiles in residential settings. In: Proceedings of the 19th ACM conference on embedded networked sensor systems. New York, NY, USA: Association for Computing Machinery; 2021, p. 520–3. http://dx.doi.org/10.1145/3485730.3494111.

[37] Bäumker E, Conrad L, Comella LM, Woias P. A fully featured thermal energy harvesting tracker for wildlife. Energies 2021;14(19):6363. http://dx.doi.org/10.3390/en14196363.

[38] Neri I, Travasso F, Mincigrucci R, Vocca H, Orfei F, Gammaitoni L. A real vibration database for kinetic energy harvesting application. J Intell Mater Syst Struct 2012;23(18):2095–101. http://dx.doi.org/10.1177/1045389X12444488.

[39] Merrett G, Yang K. EH network data repository. 2022, Engineering and Physical Sciences Research Council, EH Network Data Repository, [online] (March 2022) URL http://eh-network.org/data/.

[40] Mayer P, Magno M, Benini L. Smart power unit—mW-to-nW power management and control for self-sustainable IoT devices. IEEE Trans Power Electron 2021;36(5):5700–10. http://dx.doi.org/10.1109/TPEL.2020.3031697.

[41] Zhu C, Li X, Song L, Xiang L. Development of a theoretically based thermal model for lithium ion battery pack. J Power Sources 2013;223:155–64. http://dx.doi.org/10.1016/j.jpowsour.2012.09.035.

[42] Oldham KB. A Gouy–Chapman–Stern model of the double layer at a (metal)/(ionic liquid) interface. J Electroanal Soc 2008;613(2):131–8. http://dx.doi.org/10.1016/j.jelechem.2007.10.017.

[43] Han U, Kang H, Song J, Oh J, Lee H. Development of dynamic battery thermal model integrated with driving cycles for EV applications. Energy Convers Manage 2021;250:114882. http://dx.doi.org/10.1016/j.enconman.2021.114882.

[44] Balsamo D, Weddell AS, Merrett GV, Al-Hashimi BM, Brunelli D, Benini L. Hibernus: Sustaining computation during intermittent supply for energy-harvesting systems. IEEE Embedded Syst Lett 2015;7(1):15–8. http://dx.doi.org/10.1109/LES.2014.2371494.

[45] Michael PR, Johnston DE, Moreno W. A conversion guide: Solar irradiance and Lux illuminance. J Measur Eng 2020;8(4):153–66. http://dx.doi.org/10.21595/jme.2020.21667.